Probing spin fluctuations in NaOsO3 by muon spin rotation and NMR spectroscopy

# Probing spin fluctuations in $NaOsO_3$ by muon spin rotation and NMR spectroscopy

**Namrata Gurung[1,2], Chennan Wang[3], Nicholas S. Bingham[4], Joel A. T. Verezhak[3], Kazunari Yamaura[5], Giuseppe Allodi[6], Paola Caterina Forino[7], Samuele Sanna[7], Hubertus Luetkens [3], V. Scagnoli[1,2]**

E-mail: valerio.scagnoli@psi.ch

E-mail: s.sanna@unibo.it

[1]Laboratory for Mesoscopic Systems, Department of Materials, ETH Zurich, 8093 Zurich, Switzerland

[2]Laboratory for Multiscale Materials Experiments, Paul Scherrer Institute, 5232 Villigen PSI, Switzerland

[3]Laboratory for Muon Spin Spectroscopy (LMU), Paul Scherrer Institute (PSI), CH-5232 Villigen, Switzerland

[4]Department of Applied Physics, Yale University, New Haven, Connecticut 06511, USA

[5]International Center for Materials Nanoarchitectonics (WPI-MANA), National Institute for Materials Science, 1-1 Namiki, Tsukuba, Ibaraki 305-0044, Japan

[6]Dipartimento di Scienze Matematiche, Fisiche e Informatiche, Universit di Parma I-43124 Parma, Italy

[7]Department of Physics and Astronomy "A. Righi", University of Bologna, via Berti-Pichat 6-2, 40127 Bologna, Italy

‡

**Abstract.** We have used $\mu$SR and $^{23}$Na-NMR spectroscopic methods in the $NaOsO_3$ antiferromagnetic phase to determine the temperature evolution of the magnetic order parameter and the role of the magnetic fluctuations at the Néel temperature. Additionally, we performed muon spin relaxation measurements in the vicinity of $T_A$=30 K, where the appearance of an anomaly in the electrical resistivity was suggested to be due to a progressive reduction of the Os magnetic moment associated with spin fluctuation. Our measurements suggest the absence of prominent change in the spin fluctuations frequency at $T_A$, within the muon probing time scale and the absence of a reduction of the localized Os magnetic moment reflected by the stability within few permille of the local magnetic field strength sensed by the muons below 50 K.

‡ 29 April 2021

## 1. Introduction

The metal-insulator transition (MIT) has been a key topic of condensed matter physics since Verwey's pioneering work on magnetite [1]. Recently, interest in MITs has accelerated, due to the intriguing discovery of a new level of complexity, resulting in the presence of concurrent yet distinct phase transitions [2, 3]. In addition, progress in synthesising new materials has revealed the unexpected presence of an insulating state and MIT in several oxides containing $5d$ elements [4, 5]. Conventionally, $5d$ transition metal compounds have relatively weaker electronic correlations, favouring electron delocalization and a metallic ground state, primarily due to the larger spatial extent of the $5d$ orbitals in comparison to $3d$ orbitals. However, while the electron correlation, parametrized by the Hubbard correction term $U$, diminishes on descending the periodic table from $3d$ to $5d$ elements, the spin-orbit coupling (SOC) increases with increasing atomic number. Therefore, such materials are mostly characterized by the absence of a dominating interaction, leading to the emergence of unconventional ground states. This leads to the potential for improved theoretical understanding of complex systems as well as harvesting new physical properties to realize new devices, particularly if such systems exhibit magnetic ordering, which can be easily manipulated by an external magnetic field.

In order to benchmark the predictive power of *ab initio* calculations with experimental observations, one needs to first solve the origin of the insulating nature in magnetic $5d$ transition metal oxide systems containing Ir or Os. MITs observed in these materials have been initially argued to be of either Mott- [5, 6, 7] or Slater-type [4, 8, 9] in character. The latter mechanism proposed by Slater more than 50 years ago [10], states that the emergence of antiferromagnetic ordering opens a gap due to the folding of the Brillouin Zone that drives the system into an insulating state. This insulating state is very distinct from the metallic phase which is characterized by a paramagnetic temperature regime above the Néel ordering temperature. In the Slater model, electron correlations do not play a role, which is in direct contrast to the Mott scenario, wherein it is the electron correlations that favor the existence of an insulating ground state.

$Nd_2Ir_2O_7$, $SrIr_{0.9}Sn_{0.1}O_3$, $CaIrO_3$ and $Pb_2CaOsO_6$ were recently reported to exhibit a behaviour compatible with the Slater mechanism [11, 12, 13, 14, 15]. Similarly, $Cd_2Os_2O_7$, has been at the center of the debate on the nature of MITs, as it was first predicted to be a Slater insulator [16, 17], and later argued to undergo a smooth change in the electron density, with a gradual change in the Fermi surface, usually referred to as Lifshitz mechanism. [18, 19]

Amongst $5d$ materials, $NaOsO_3$ is perhaps the one that has received the most attention thus far [4, 8, 20, 9, 21, 22, 23], due to the concomitant observation of magnetic ordering and an abrupt change in the resistivity. [4] Specifically, $NaOsO_3$ undergoes a metal-insulator transition and antiferromagnetic ordering at the same temperature, $T_{\mathrm{MIT}} = T_{\mathrm{N}} = 410$ K. The magnetic moment determined by neutron diffraction refinement is $1\,\mu_B$, indicative of the coexistence of localized and itinerant magnetism [8]. Below $T_{\mathrm{N}}$, magnetic moments order almost parallel to the c-axis in a G-type antiferromagnet with a very small ($< 0.01\ \mu_{\mathrm{B}}$) ferromagnetic component along the b-axis. The concomitant MIT, antiferromagnetic ordering and the absence of crystallographic symmetry breaking [8, 9] are suggestive of a magnetically driven MIT. However, due to the presence of energetically similar competing interactions, a consensus on the nature of the metal-insulator mechanism operating in this perovskite

is absent.

Current literature on $NaOsO_3$ includes pressing arguments for different variations of MIT, namely; 1) the aforementioned Slater mechanism [4, 8, 9], 2) the Mott-Hubbard mechanism [20] in which the MIT is independent of magnetic correlations and is only the result of an electron localization effect controlled by an on-site strong Coulomb interactions, 3) a MIT described as close to but not within either Heisenberg limit or Slater limit [22, 23], and 4) a Lifshitz MIT [21] in which the continuous MIT is attributed to a continuous reconstruction of the Fermi surface, strongly linked to the presence of directional spin fluctuations. It is therefore desirable to perform further experiments to ascertain which model describes best the MIT in $NaOsO_3$.

Within this latter model, the double anomaly behavior in the resistivity curve at $T_{\rm N} = 410$ K and $T_{\rm A} = 30$ K (see Figure 2a of Ref. [4]) is explained by the temperature evolution of transverse (rotational) and longitudinal (amplitude) spin fluctuations and their effect on the $NaOsO_3$ band structure [21]. Namely, at low temperatures, $NaOsO_3$ is an antiferromagnetic insulator with an Os magnetic moment $\mu_{Os} = 1.17\ \mu_B$ for T=0 K. Upon increasing the temperature above $T_{\rm A}$, the system enters a pseudogap bad-metal regime due to the presence of longitudinal spin fluctuations (at $T_{\rm A}$ it is predicted $\mu_{Os} = 1.15\ \mu_B$, a 1.5 % reduction over the 0 K value). Finally, at $T_{\rm N}$, the onset of rotational spin fluctuations facilitate the closure of the insulating pseudogap and the system becomes metallic, but with an unexpected weak Curie-Weiss paramagnetic behavior. It is therefore desirable to perform further experiments to ascertain which model describes best the MIT in $NaOsO_3$.

## 2. Experimental Details

In this paper we present experimental results obtained by performing muon spin rotation ($\mu$SR) and nuclear magnetic resonance (NMR) measurements performed on $NaOsO_3$ polycristalline samples, grown as described in [4].

Muon spin rotation spectroscopy experiments on a 5 mm diameter polycrystalline pellet were performed on the GPS spectrometer at the Swiss Muon Source at the Paul Scherrer Institute [24]. The surface muons produced at the target with $> 95\%$ spin polarization are implanted in the sample. Muons thermalize rapidly to the preferential sites of the crystal lattice with the preserved initial muon polarization. As our sample is small as compared with the beam spot size, the detection scheme of the spectrometer was set to the veto-mode, to ensure the background positron events generated by the muons missing the small sample is less than a few percent in the total asymmetry. The measurements above the room temperature were performed with the sample placed on a thin copper foil with the Apiezon® grease H to ensure good thermal contact. During the measurement in zero field (ZF), the residual magnetic field was actively compensated below 0.02 Oe at the sample position. The measured $\mu$SR spectrum was analyzed with `musrfit` package [25]. To analyze the slow relaxing tail of the muon spectra, we adopted the single histogram fit method for directly fitting our muon depolarization model to the positron histograms, allowing each detector efficiency to be treated independently. The positron histogram on the $j$-th detector $N_j(t)$ is given by:

$$N_j(t) = N_{0,j} e^{-t/\tau_\mu} [1 + A_{0,j} P_j(t)] + N_{{\rm bkg},j}. \quad (1)$$

Here, $N_{0,j}$ is the measured muon decay events at $t$=0. The exponential term accounts for the radioactive decay of muon ensemble. $A_{0,j}$ is the instrumental asymmetry of

detector pairs. $P_j$ is the projection of muon depolarization on the respected detector pairs. $N_{\mathrm{bkg},j}$ accounts for the background events of each detector.

The $^{23}$Na NMR experiments were performed by means of a home-built phase-coherent spectrometer [26] in an applied field of = 7.95 T, with a nitrogen-flow cryostat (in the 80-350 K temperature range) or a small oven (350-440 K) as sample environments. The sample, finely ground in order to minimize eddy currents induced by the rf field, was placed in the coil of a lumped LC resonator hosted by the cryostat or oven, tuned at the working frequency by a servo-assisted automatic system plugged-in into the spectrometer. Spectral data were collected point by point at discrete frequencies by exciting spin echoes by a standard $P-\tau-P$ pulse sequence, with equal rf pulses $P$ of duration $\approx 4$ $\mu$s and intensity optimized for maximum signal, and delays $\tau \approx 10$ $\mu$s. The spectra were reconstructed by merging the discrete Fourier transforms of the spin echo signals, phase-corrected to yield positive-definite absorption lines and frequency-shifted relative to one another by the offset of the spectrometer reference frequency, in a variant of the procedure described in [27].

## 3. Results and Discussion

### *3.1. Muon spin rotation ($\mu$SR)*

In this section, we firstly address the relevance of the proposed Lifshitz mechanism implying the appearance of substantial spin fluctuations at $T_{\mathrm{A}}$, by $\mu$SR experiments. In a polycrystalline sample with magnetic order, the direction of the internal static magnetic field sensed by the implanted muon ensemble is distributed equally probable along all directions. On average, 1/3 of the total internal field will be projected in parallel to the initial muon spin direction and 2/3 in perpendicular. In such case, the zero field (ZF) muon depolarization function is described as:

$$P_z(t) = f_m\Big\{\frac{2}{3}\Big[\sum_{i=1}^{n} f_i \cos(\gamma_\mu \langle B_{\mu,i}\rangle t) e^{-(\sigma_i^2 t^2)/2} + f_s e^{-\lambda_s t}\Big] + \frac{1}{3} e^{-\lambda_L t}\Big\} + (1 - f_m), \tag{2}$$

where $\gamma_\mu$ is the muon gyromagnetic ratio ($= 2\pi \times 135.53\,\mathrm{MHz/T}$) and $f_m$ is the magnetic volume fraction. The oscillatory term with a fraction $f_i$ describes the static long-range magnetic ordering, where $i$ indicates the corresponding muon stopping site. The distribution of static internal field at each muon site, $B_{\mu,i}$, is approximated by a Gaussian distribution associated with the depolarization rate $\sigma_i$ [28, 29]. The possible contribution of a state with strongly disordered moments without forming long-range magnetic order is accounted for by an exponential decay term with a volume fraction $f_s$ and an exponential depolarization rate $\lambda_s$. Assuming this inhomogeneous static magnetic phase is fully static at low temperatures, only the static relaxation part needs to be taken into account. The sum of the dynamical fluctuations contributed by all muon sites is accounted by a single exponential function with muon depolarization rate $\lambda_L$, also known as the longitudinal depolarization rate. Finally, (1-$f_m$) accounts for paramagnetic contribution from the non-magnetic minority phase or instrument background.

The results obtained from ZF experiments are presented in figure 1. The sample shows a full magnetic volume fraction below $T_{\mathrm{N}}$ whereas the instrumental background is about 5%. The fitting results reveals the presence of three different muon stopping

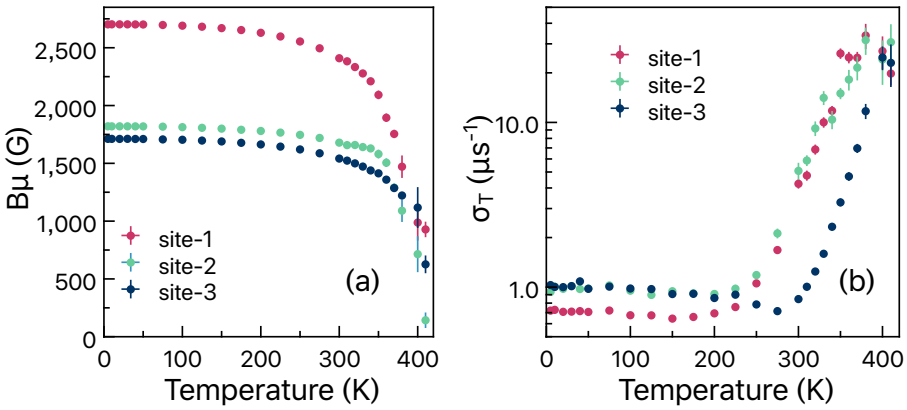


**Figure 1.** Temperature dependence of (a) the magnitude and (b) the broadening of the local magnetic field at the three different muon stopping sites determined from the zero field $\mu$SR data.

sites, as reported on isostructural perovskite compounds [30, 31]. The fraction of each muon site in the long-range ordered magnetic phase is 33.3% (site-1), 25.9% (site-2) and 27.8% (site-3), and the fraction of the inhomogeneous magnetic region is about 13%, which may be due to the presence of an additional muon site with a disordered magnetic ordering. Meanwhile, a temperature independent behavior is observed for these fractions. As presented in figure 1(a), below $T_{\rm N}$ the internal field of the magnetically ordered volume increases rapidly, and the saturation occurs around 200 K. The highest local magnetic field strength appeared at the muon site-1 suggests the strongest coupling between the muon and the local magnetic moment. The local magnetic field strength $B_\mu$ is proportional to the Os magnetic moment, at least with first approximations. We observe that the estimated $B_\mu$ mean value for site-1 at temperatures below 50 K is $B_{\mu,1}$ =2702.0(5) G with a standard deviation of less than 0.05%. A similar standard deviation is found also for $B_{\mu,2}$ and $B_{\mu,3}$. It therefore can be concluded that the (localized) Os magnetic moment is showing no significant variation in this temperature range and start to decrease only above 50 K. Additionally, the temperature dependence of the quantity $B_G$=$B_\mu$(0)-$B_\mu$(T) can be used to infer the presence of a gap in the the spin wave spectrum [32]. $B_G$ follows a $T^{3/2}e^{-E_G/k_BT}$ temperature dependence rather than a Bloch power law when approaching zero temperature. Such behaviour indeed indicates the presence of a gap $E_G$ in the spin wave spectrum [32], consistent with the reports from [33].

Finally we note that we observe a temperature dependent lineshape broadening associated with inhomogeneous field distribution towards $T_{\rm N}$, as illustrated in figure 1(b). However, the reduction of the linewidth above 350 K is likely due to the motional narrowing as a result of thermally activated muon hopping [34, 35].

To unambiguously identify the muon depolarization due to the dynamical spin fluctuations, a weak longitudinal magnetic field (LF) $B_{LF}$=50 Oe was applied along the muon initial polarization to decouple static internal fields due to the presence of impurity phases. This low static field $B_{LF}$ has no effect on the longitudinal fraction of the $\mu$SR signal: neither on its amplitude, since $B_{LF} << B_\mu$ nor it affects the longitudinal relaxation rate, which depends only on the internal field dynamics.

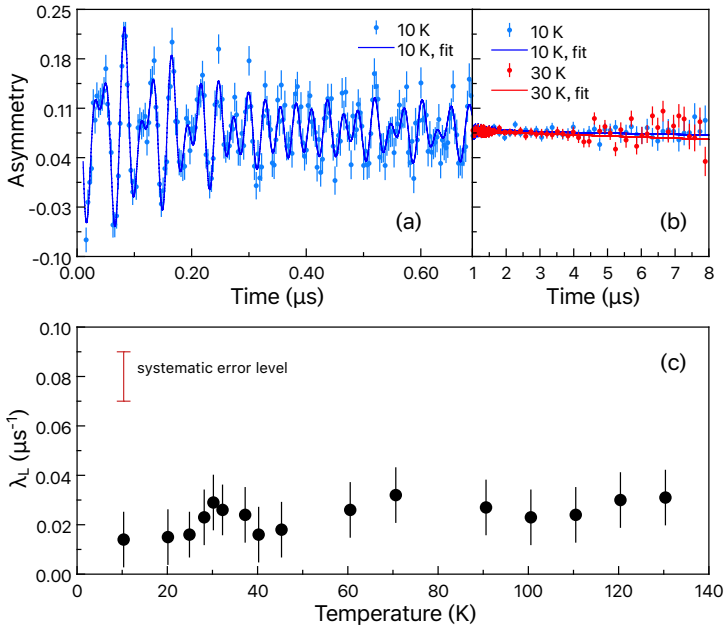


**Figure 2.** (a) Selected region of $\mu$SR time spectra of $NaOsO_3$ polycrystalline sample in LF = 50 Oe at 10 K fitted with a model based on (2). (b) Comparison of the measured $\mu$SR time spectra at 10 K and 30 K and the corresponding fitting result. (c) Temperature dependence of the longitudinal relaxation rate $\lambda_L$. The scale of the systematic error of $1\sigma$ indicates our estimated measurement accuracy limit for the determined relaxation rate.

The results of our weak LF $\mu$SR measurements are presented in figure 2. The time spectra were analyzed with the single histogram fit for the forward and backward positron detectors. A fit to the experimental data are presented in the top panels of figure 2. In the short time scales, the observed oscillatory signal is contributed by the local internal field sensed by three muon sites as mentioned earlier. At longer time scales, the exponential decay associated with the 1/3 component of (2) reflects the presence of spin fluctuations [36]. As shown in figure 2(c), the observed dynamical muon depolarization rate $\lambda_L$ is close to the accuracy limit of our experiments (0.02 $\mu s^{-1}$) [37] and stays constant within the measurement uncertainty in the temperature range up to 200 K. No evidence of a consistent development of low energy spin dynamics is clearly evidenced above $T_A$, at least within the characteristic muon detection time window (corresponding spin fluctuation rate $\nu = 0.1$ MHz - 1 THz). Our data indicates that the existence of significant spin fluctuations on a MHz frequency scale can be excluded in this temperature range.

Furthermore, the ZF data fitted with (2) provides an estimation of the local magnetic field strength at the muon stopping site as well as an estimation of the degree of long-range ordering in the sample. The extracted temperature dependence of the magnetic order parameter, namely the staggered magnetization, is plotted in figure 3, despite the muon diffusion may hinder an accurate determination of the temperature dependence of $B_\mu$ above 350 K.

Summarizing, our low temperature $\mu$SR results indicate the absence of spin

fluctuations within the muon detection window and the steadiness of the staggered magnetization. It appears therefore that the resistivity anomaly occurring at $T_A$ is not related to any change in the $NaOsO_3$ magnetic structure. Possibly, a thermally driven increase of the unoccupied states population lying close to the ground state rather than a reduction of the Os magnetic moment would be at the origin of the smooth temperature evolution of the band structure leading to appearance of a Fermi surface at $T_A$ as suggested by Kim *et al.* [21].

### *3.2. $^{23}$Na Nuclear Magnetic Resonance (NMR)*

In order to ascertain the temperature behavior of the order parameter and of the relaxation rate at high temperatures, we have performed complementary $^{23}$Na NMR measurements at $\mu_0 H = 7.95$ T in the temperature range 80 K $< T <$ 440 K. By modelling the $^{23}$Na NMR spectra as described in the Appendix, we quantified the contribution arising from the AFM and weak FM components. They are proportional to the second moment (approximately given by the spectral width) and the first moment (corresponding approximately to the isotropic term of the frequency shift of the resonance) of the powder distribution of the internal fields, hereafter $B_{\mathrm{AFM,NMR}}$ and $B_{\mathrm{FM,NMR}}$ respectively. Neighbouring Os spins sit in nearly symmetric positions with respect to the Na nucleus, resulting in a $^{23}$Na NMR signal which is weakly coupled to the large AFM component and strongly to the weak FM one. The temperature behavior of both the antiferromagnetic (AFM) and ferromagnetic (FM) components around $T_N$ is displayed in the inset of figure 3 with a fit using a power-law expression $B_{\mathrm{NMR}} \propto (1 - T/T_N)^{\beta}$. The fit yields a magnetic transition temperature $T_N$=410.1(2) K, in agreement with values reported in the literature, and a critical exponent $\beta$=0.53(3) close to 1/2, which coincides with the value expected for a mean field behavior.

The main panel of figure 3 shows the behavior of the $B_{\mathrm{AFM,NMR}}$ in comparison to the internal field at the three different muon sites $B_\mu$=$B_{\mu,i}$ (normalized to their respective low temperature values). By comparing their temperature dependence with the results obtained with NMR, it is clear that muon diffusion starts to be activated already above 250 K and none of the $B_{\mu,i}$ has a temperature dependence which follows $B_{\mathrm{AFM,NMR}}$.

To gain more insight into the magnetic dynamics occurring at the MIT, we have also measured the $^{23}$Na NMR spin-lattice relaxation rate $1/T_1$ in the temperature range 150 K $< T <$ 450 K, which is displayed in figure 4. Above the magnetic transition temperature the data show that the $1/T_1T$ is almost constant (see inset), reflecting the behavior expected for a metal [38]. While crossing the MIT a steep increase and a sudden reduction in $1/T_1T$ is observed. Two main features can be noticed: the maximum is clearly below $T_N$ and the temperature dependence resembles a lambda transition rather than a cusp. These features indicate that the observed peak is not merely due to the critical fluctuations, typically maximised at $T_N$, as expected for a second order magnetic phase transition. Such unexpected results can be qualitatively explained, to the aforementioned weak coupling of the $^{23}$Na nuclei with the AFM order parameter, and by observing that the observed $1/T_1T$ temperature dependence is likely related to the metal-insulator phase transition. The change of the electronic behavior around the magnetic transition is also reflected by the dramatic change in the hyperfine coupling of the $^{23}$Na nucleus to the uniform component (wave vector q=0) of the magnetization as displayed in the Jaccarino plot of Figure 6. Therefore,

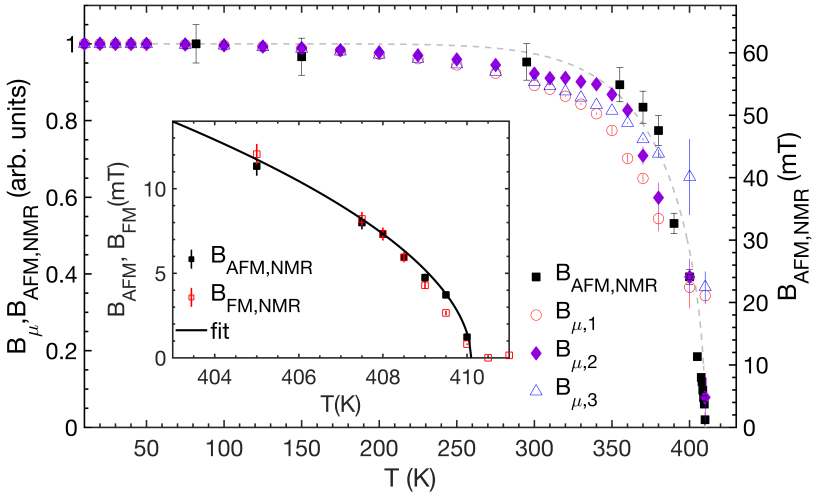


**Figure 3.** Temperature dependence of the internal fields, proportional to the magnetic order parameter, at the muon site, $B_{\mu,i}$, and at the Na position, $B_{NMR}$ (square), as detected from $\mu$SR and NMR, respectively. Dashed line is a guide to the eye. The inset illustrates the FM (open) and AFM (close) contributions to the internal field in the vicinity of the phase transition, as determined by NMR. Solid line is a fit of the temperature dependence in the vicinity of $T_N$ as described in the text.

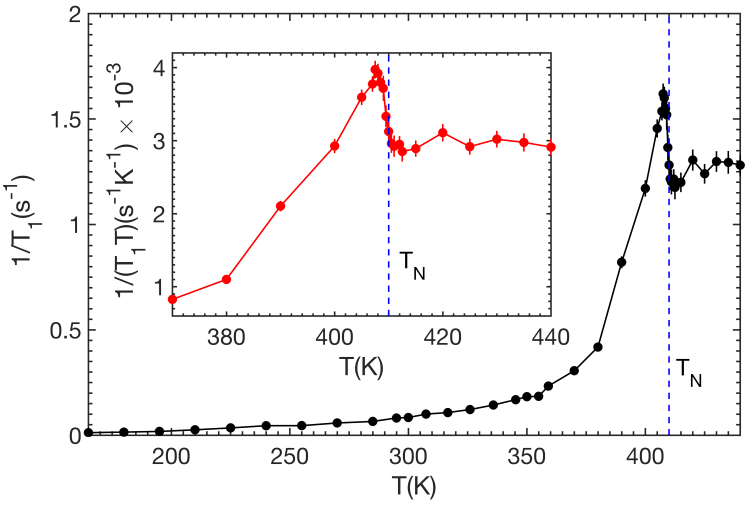


**Figure 4.** Temperature dependence of the relaxation rate $1/T_1$, as measured from $^{23}$Na NMR measurements with $\mu_0 H = 7.95$ T. The inset illustrates $1/T_1T$. The dotted line indicates the temperature corresponding to $T_N$, as determined from the analysis of the NMR spectra acquired during the same $1/T_1$ measurements.

our results suggest that $T_{MI}$ and $T_N$ might not coincide. In this respect, it would be interesting to compare such results with NMR studies on other materials that show a

MIT occurring concurrently with AFM ordering.

## 4. Conclusions

In summary, via $\mu$SR spectroscopic method, we have shown that the resistivity anomaly behavior ($T_A$ = 30 K) is not associated with any magnetic-related feature within the muon frequency window. We find no evidence of a peak in the muon relaxation rate and of the presence of a temperature dependence of the magnetic field at the muon site $B_\mu$. Such results indicate that no low energy spin fluctuations (< 1 THz) nor a variation of the staggered magnetization, proportional to the Os magnetic moment, occur at $T_A$.

Therefore, the mechanism based on the development or existence of longitudinal spin fluctuation proposed in [21] seems not applicable to $NaOsO_3$ below 50 K. However, a smooth temperature evolution leading to the appearance of band crossing at the Fermi level as suggested by Kim et al. [21], could be explained by alternative mechanisms. As an example, such change could be induced by the thermally driven increase in the unoccupied states population lying close to the ground state. Finally, complementary NMR experiments reveal a dramatic change in the hyperfine coupling of the $^{23}$Na nucleus to the uniform component of the magnetization at $T_N$ and suggests that $T_{MI}$ and $T_N$ might not coincide.

## Acknowledgements

The muon raw data are available from the S$\mu$S online database [39]. Further raw data files that support this study are available via the Zenodo repository [10.5281/zenodo.4452113 link will be activated]. We thank R. De Renzi, P. Carretta, V. Mitrovic and G. Simutis for fruitful discussions. This research work was supported from funding provided by the Swiss National Science Foundation, SNF Project No. 200021_162863. Work in Japan was supported by JSPS KAKENHI Grant No. JP20H05276, and Innovative Science and Technology Initiative for Security (Grant No. JPJ004596), ATLA, Japan.

## Appendix

*Modelling of the $^{23}$Na Nuclear Magnetic Resonance data*

Spin lattice relaxation rates were determined from the recovery of the longitudinal nuclear spin polarization following the saturation of central portion of the spectrum by an aperiodic train of 6-8 pulses. In the case of a nuclear $I = 3/2$ spin like $^{23}$Na, a two-exponential recovery of the amplitude of the central transition $m = 1/2 \leftrightarrow -1/2$ is predicted by rate equations for the nuclear populations,

$$A_0(t) = A_0^{(0)} \left[ \alpha \left( 1 - e^{-t/T_1} \right) + (1 - \alpha) \left( 1 - e^{-6t/T_1} \right) \right]. \quad (3)$$

where the relative weight $\alpha$ depends on the initial state of the spin system following saturation. Two limiting cases can be modeled, i.e. a complete and a "fast" saturation of the central line, yielding $\alpha = 0.4$ and $\alpha = 0.1$, respectively. [40, 41] Such ideal cases, however, can be hardly attained experimentally, and the best fit of the data was actually obtained by an intermediate $\alpha$ value, which was left fixed across temperatures.

The broad and complex $^{23}$Na NMR spectra of polycrystalline $NaOsO_3$ (figure 5) are the result of the powder average of both magnetic and quadrupolar interactions of the $^{23}$Na nucleus, of comparable magnitude in the ordered phase. The minimal model capable of reproducing the spectra both above and below $T_N$ includes the following terms, some of which can be straightforwardly interpreted as the antiferromagnetic (AF) and ferromagnetic (FM) order parameters as probed by NMR.

In the total nuclear spin Hamiltonian $\mathcal{H} = \mathcal{H}_Z + \mathcal{H}_Q$, the Zeeman component is written as

$$\mathcal{H}_Z = \hbar\gamma\vec{B}_{\text{nuc}} \cdot \mathbf{I} = \hbar\gamma \left[\left(1 + \hat{K}\right) \mu_0\vec{H}_0 + \vec{B}_{\text{int}}\right] \cdot \mathbf{I} \tag{4}$$

where $\mathbf{I}$ is the nuclear spin, $\hat{K}$ is the Knight shift tensor, $\vec{B}_{\text{int}}$ is the internal field at the nucleus, hyperfine in origin, and $\gamma/2\pi = 11.263$ MHz/T is the gyromagnetic ratio of $^{23}$Na.

The $\vec{B}_{\text{int}}$ term is treated as a constant magnetic field with well defined magnitude and direction with respect to the crystal, independent of the direction of the applied field. Such a *rigid* internal field, adding up undistorted to the external one, corresponds to the model of a hard magnet with zero susceptibility, i.e. an ideal antiferromagnet. Therefore $\vec{B}_{\text{int}}$ may be identified with the AF order parameter as seen from NMR. Its non-zero value arises from a slight deviation of the Na site from a local cubic symmetry, which would otherwise lead to a vanishing net transferred hyperfine field at the center of an osmium spin octet ordered in a G-type AF structure. Due to the fact that the hyperfine couplings of $^{23}$Na are largely canceled out, $\vec{B}_{\text{int}}$ is expected to be relatively small, despite the AF component of the magnetic structure is overwhelmingly larger than the weak FM moment.[4] On its own, a rigid $\vec{B}_{\text{int}}$ would yield an NMR lineshape

$$g(\omega) = \begin{cases} \dfrac{\omega}{2\gamma^2\mu_0 H_0 B_{\text{int}}} \approx \dfrac{1}{2\gamma B_{\text{int}}} & \text{for} \quad -\gamma B_{\text{int}} < \omega - \gamma\mu_0 H_0 < \gamma B_{\text{int}} \\ \\ 0 & \text{elsewhere} \end{cases}$$

when averaged over the random orientation of the crystal relative to the external field, yielding a second moment $\Delta\omega^2 \approx \gamma^2 B_{\text{int}}^2/3$. The latter is expected to be the dominant contribution to the magnetic linewidth below $T_N$.

The finite susceptibility of the material is accounted for by a Knight shift $\Delta H = \hat{K}\vec{H}_0$. The Knight shift tensor $\hat{K}$ is proportional to the spin susceptibility via the hyperfine coupling:

$$\hat{K} = \frac{1}{\gamma g \mu_B N_A} \left( \sum_{j \in \text{n.n.}} \hat{\mathcal{B}}_j \right) \hat{\chi}_{\text{dc}} \tag{5}$$

where $\hat{\mathcal{B}}_j$ is the hyperfine coupling constant of the Na nucleus with its $j$-th nearest neighbor Os spin, and $\hat{\chi}_{\text{dc}}$ is the molar dc susceptibility tensor, defined in terms of the macroscopic molar magnetization $M$ and the applied field by the relation $\vec{M} = \hat{\chi}_{\text{dc}}\vec{H}_0$. Both the linear response of the magnetic moment $M$ in $H_0$ (i.e. the differential susceptibility $\chi = \partial M/\partial H$) and the weak FM moment, which aligns along $\vec{H}_0$ but whose magnitude is independent of the intensity of the magnetic field, contribute to $\chi_{\text{dc}}$ as defined above, hence to $\hat{K}$ as well. These two contributions, of comparable magnitude in an applied field of $\approx 7.95$ T, [4] might be unraveled in principle by measuring the NMR spectra in different applied fields, which was not possible with our magnet. The isotropic Knight shift component $K_{\text{iso}} = 1/3\,\text{Tr}\,(\hat{K})$ yields an overall shift of the powder spectrum, proportional to the net magnetic

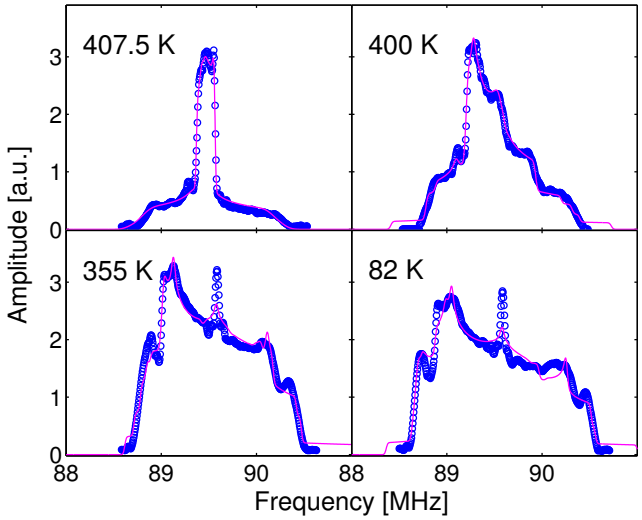


**Figure 5.** Representative $^{23}$Na NMR spectra in the 80-410 K temperature range, in an applied field of $\approx 7.95$ T. The solid lines superimposed to open symbols are fits to the model described in the text.

moment (either paramagnetic of weakly FM), and is our NMR determination of the so-called FM order parameter. Powder average of the traceless component $\hat{K} - K_{\rm iso}$, on the other hand, produces additional inhomogeneous broadening of the spectra, though to a lesser extent than $B_{\rm int}$.

In a frame of reference of the crystal, the quadrupolar interaction of $^{23}$Na (nuclear spin $I = 3/2$) is written as

$$\mathcal{H}_Q = \frac{h\nu_Q}{6}\left[3I_z^2 - I\left(I+1\right) + \frac{\eta}{2}\left(I_+^2 + I_-^2\right)\right] \tag{6}$$

where the quadrupolar frequency $\nu_Q$ is defined in terms of the nuclear quadrupole moment $Q$ and the main component $V_{zz}$ of the electric field gradient (EFG) tensor as $\nu_Q = 3eV_{zz}Q/[2hI(2I-1)]$, $x$, $y$ are the other EFG principal axes, and $\eta = \left||V_{yy}| - |V_{xx}|\right|/V_{zz}$ is the EFG rhombicity factor. [38] In a large magnetic field $B_{\rm nuc} \gg 2\pi\nu_Q/\gamma$, $\mathcal{H}_Q$ can be treated as a perturbation of $\mathcal{H}_Z$. Closed-form perturbative expressions for the $2I$ Zeeman transitions, whose degeneracy is resolved by $\mathcal{H}_Q$, can be calculated up to second order in $\nu_Q/(\gamma H_0)$. [42] The central transition $m = 1/2 \leftrightarrow -1/2$, unaffected by the EFG to first perturbation order, yields the sharper central line, while satellite transitions $m = \pm 1/2 \leftrightarrow \pm 3/2$, strongly angle dependent, produce a broad shoulder in the spectrum with powder singularities. Such features are clearly visible close to and above $T_N$ (Figure 5), where the quadrupolar interaction is the leading source of line broadening.

The powder spectra resulting from the average of the Zeeman transitions of $\mathcal{H} = \mathcal{H}_Z + \mathcal{H}_Q$ over crystal orientation was calculated numerically after an algorithm by Alderman et al.[43] No constraint was imposed on either $\vec{B}_{\rm int}$ or $\hat{K}$, whose orientations were left independent of each other and of the EFG axes. Thus, $\vec{B}_{\rm int}$ was parametrized by its magnitude and two polar angles relative to the crystal frame, and $\hat{K}$ by $K_{\rm iso}$, two traceless components and three Euler angles. Gaussian line broadening was also allowed for to mimic inhomogeneities of the interactions. The good qualitative

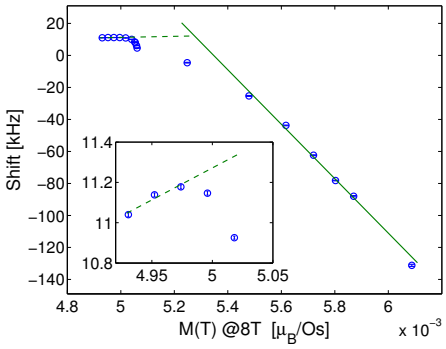


**Figure 6.** Evolution of coupling of the $Na^{23}$ nucleus with the net Os magnetic moment in the vicinity of the phase transition. The inset is a blow-up in the paramagnetic region ($T \geq 420$ K).

agreement of the model with data is illustrated by Figure 5, showing some selected spectra and their fitting curves.

Fits of the spectra to the model provided consistent values and smooth temperature dependencies of their free parameters throughout the whole temperature range. The internal field $B_{\rm int}$ is plotted vs $T$ in Figure 2 of the main paper, referred to therein as $B_{AF,NMR}$ owing to its physical meaning as AF order parameter (see above). The absolute shift of the NMR spectrum $\Delta\nu = (\gamma/2\pi)\, K_{\rm iso}\mu_0 H_0$ ($\Delta B = K_{\rm iso}\mu_0 H_0$ in field units, referred to as $B_{FM,NMR}$ in the inset of Figure 2), is plotted in Figure 6 as a function of the net magnetic moment measured by magnetometry in the same magnetic field $\mu_0 H_0 \approx 7.95$ T employed for NMR measurements (Jaccarino plot), with temperature 405 K $\leq T \leq$ 440 K as the implicit parameter. Following the above discussion and Eq. 5, the two quantities are proportional to each other except for small temperature independent orbital terms in either $K$ or $\chi$. A plot of $\Delta\nu$ vs $M$ is therefore expected to yield a straight line with slope $\partial\nu/\partial M$ equal to the hyperfine coupling constant (in suitable units) both above and below the ordering temperature, a behavior actually observed in all conventional magnets.

Figure 6, on the contrary, shows a dramatic change in the net coupling constant $\mathcal{B}_{\rm tot} = \sum_j \mathcal{B}_j$ across the magnetic transition, from a small positive value $\mathcal{B}_{\rm tot} \approx 3$ MHz/$\mu_B$ well above $T_N$ (smallest $M$ values in the figure) to a much larger and negative value $\mathcal{B}_{\rm tot} = -170 \pm 10$ MHz/$\mu_B$ at $T < T_N$. The step in $\mathcal{B}_{\rm tot}$ indicates the occurrence of an electronic transition across $T_N$, with larger degree of covalency and a stronger transfer of spin polarization from Os ions to Na nuclei in the ordered phase.

## References

[1] Verwey E 1939 *Nature* **144** 327
[2] McLeod A S, van Heumen E, Ramirez J G, Wang S, Saerbeck T, Guenon S, Goldflam M, Anderegg L, Kelly P, Mueller A, Liu M K, Schuller I K and Basov D N 2017 *Nat. Phys.* **13** 80–86
[3] Post K W, McLeod A S, Hepting M, Bluschke M, Wang Y, Cristiani G, Logvenov G, Charnukha A, Ni G X, Radhakrishnan P, Minola M, Pasupathy A, Boris A V, Benckiser E, Dahmen K A, Carlson E W, Keimer B and Basov D N 2018 *Nat. Phys.* **14** 1056–1061
[4] Shi Y G, Guo Y F, Yu S, Arai M, Belik A A, Sato A, Yamaura K, Takayama-Muromachi E, Tian H F, Yang H X, Li J Q, Varga T, Mitchell J F and Okamoto S 2009 *Phys. Rev. B* **80**(16) 161104

[5] Kim B J, Jin H, Moon S J, Kim J Y, Park B G, Leem C S, Yu J, Noh T W, Kim C, Oh S J, Park J H, Durairaj V, Cao G and Rotenberg E 2008 *Phys. Rev. Lett.* **101**(7) 076402

[6] Sala M M, Boseggia S, McMorrow D F and Monaco G 2014 *Phys. Rev. Lett.* **112** 026403

[7] Chapon L and Lovesey S 2011 *J. of Phys.: Cond. Matt.* **23** 252201

[8] Calder S, Garlea V O, McMorrow D F, Lumsden M D, Stone M B, Lang J C, Kim J W, Schlueter J A, Shi Y G, Yamaura K, Sun Y S, Tsujimoto Y and Christianson A D 2012 *Phys. Rev. Lett.* **108**(25) 257209

[9] Gurung N, Leo N, Collins S P, Nisbet G, Smolentsev G, García-Fernández M, Yamaura K, Heyderman L J, Staub U, Joly Y, Khalyavin D D, Lovesey S W and Scagnoli V 2018 *Phys. Rev. B* **98**(11) 115116

[10] Slater J 1951 *Phys. Rev.* **82** 538

[11] Nakayama M, Kondo T, Tian Z, Ishikawa J J, Halim M, Bareille C, Malaeb W, Kuroda K, Tomita T, Ideta S, Tanaka K, Matsunami M, Kimura S, Inami N, Ono K, Kumigashira H, Balents L, Nakatsuji S and Shin S 2016 *Phys. Rev. Lett.* **117**(5) 056403

[12] Cui Q, Cheng J G, Fan W, Taylor A E, Calder S, McGuire M A, Yan J Q, Meyers D, Li X, Cai Y Q, Jiao Y Y, Choi Y, Haskel D, Gotou H, Uwatoko Y, Chakhalian J, Christianson A D, Yunoki S, Goodenough J B and Zhou J S 2016 *Phys. Rev. Lett.* **117**(17) 176603

[13] Singh V and Pulikkotil J J 2016 *Phys. Chem. Chem. Phys.* **18**(37) 26300–26305

[14] Kim S W, Liu C, Kim H J, Lee J H, Yao Y, Ho K M and Cho J H 2015 *Phys. Rev. Lett.* **115**(9) 096401

[15] Jacobsen H, Feng H L, Princep A J, Rahn M C, Guo Y, Chen J, Matsushita Y, Tsujimoto Y, Nagao M, Khalyavin D, Manuel P, Murray C A, Donnerer C, Vale J G, Sala M M, Yamaura K and Boothroyd A T 2020 *Phys. Rev. B* **102**(21) 214409

[16] Mandrus D, Thompson J R, Gaal R, Forro L, Bryan J C, Chakoumakos B C, Woods L M, Sales B C, Fishman R S and Keppens V 2001 *Phys. Rev. B* **63**(19) 195104

[17] Padilla W J, Mandrus D and Basov D N 2002 *Phys. Rev. B* **66**(3) 035120

[18] Hiroi Z, Yamaura J, Hirose T, Nagashima I and Okamoto Y 2015 *APL Mater.* **3** 041501

[19] Koda A, Hirose H T, Miyazaki M, Okabe H, Hiraishi M, Yamauchi I, Kojima K M, Nagashima I, Yamaura J, Hiroi Z and Kadono R 2019 *Phys. Rev. B* **100**(24) 245113

[20] Middey S, Debnath S, Mahadevan P and Sarma D 2014 *Phys. Rev. B* **89** 134416

[21] Kim B, Liu P, Ergönenc Z, Toschi A, Khmelevskyi S and Franchini C 2016 *Phys. Rev. B* **94**(24) 241113

[22] Vale J G, Calder S, Donnerer C, Pincini D, Shi Y, Tsujimoto Y, Yamaura K, Sala M M, Van den Brink J, Christianson A D *et al.* 2018 *Phys. Rev. Lett.* **120** 227203

[23] Vale J G, Calder S, Donnerer C, Pincini D, Shi Y, Tsujimoto Y, Yamaura K, Sala M M, van den Brink J, Christianson A *et al.* 2018 *Phys. Rev. B* **97** 184429

[24] Amato A, Luetkens H, Sedlak K, Stoykov A, Scheuermann R, Elender M, Raselli A and Graf D 2017 *Rev. Sci. Instrum.* **88** 093301

[25] Suter A and Wojek B 2012 *Phys. Procedia* **30** 69 – 73 12th International Conference on Muon Spin Rotation, Relaxation and Resonance (SR2011)

[26] Allodi G, Banderini A, De Renzi R and Vignali C 2005 *Rev. Sci. Instrum.* **76** 083911

[27] Clark W G, Hanson M E, Lefloch F and Sgransan P 1995 *Rev. Sci. Instrum.* **66** 2453–2464

[28] de Réotier P D and Yaouanc A 1997 *J. Phys. Cond. Matter* **9** 9113–9166

[29] Smidman M, Adroja D T, Hillier A D, Chapon L C, Taylor J W, Anand V K, Singh R P, Lees M R, Goremychkin E A, Koza M M, Krishnamurthy V V, Paul D M and Balakrishnan G 2013 *Phys. Rev. B* **88**(13) 134416

[30] Holzschuh E, Denison A B, Kündig W, Meier P F and Patterson B D 1983 *Phys. Rev. B* **27**(9) 5294–5307

[31] Heffner R H, Sonier J E, MacLaughlin D E, Nieuwenhuys G J, Luke G M, Uemura Y J, Ratcliff W, Cheong S W and Balakrishnan G 2001 *Phys. Rev. B* **63**(9) 094408

[32] Jaccarino V 1965 *Nuclear Resonance in Antiferromagnets* vol IIa (New York: Academic Press) p 322

[33] Calder S, Vale J G, Bogdanov N, Donnerer C, Pincini D, Moretti Sala M, Liu X, Upton M H, Casa D, Shi Y G, Tsujimoto Y, Yamaura K, Hill J P, van den Brink J, McMorrow D F and Christianson A D 2017 *Phys. Rev. B* **95**(2) 020413

[34] Denison A B 1984 *J. Appl. Phys.* **55** 2278–2283

[35] Keren A, Le L P, Luke G M, Sternlieb B J, Wu W D, Uemura Y J, Tajima S and Uchida S 1993 *Phys. Rev. B* **48**(17) 12926–12935

[36] Yaouanc A and Dalmas de Reotier P 2011 *Muon spin rotation, relaxation, and resonance: applications to condensed matter* International series of monographs on physics (Oxford: Oxford Univ. Press) URL `https://cds.cern.ch/record/1385534`

[37] The absolute accuracy of the determination is given by experimental systematic errors (i.e. background determination, zero field compensation, potentially unsuitable fitting model, etc.). In addition also includes the temporal stability of the instrument and beamline on the longer period. This includes proton beam / muon beam position stability (power supplies, thermal drifts, corrections of proton beam position) and therefore beam spot stability at the instrument, temporal stability of $\mu$SR data acquisition (i.e. electronics, temporal stability of magnetic fields in the experimental hall, etc.) All in all, this temporal variation of the timescale of hours, the estimated actual measurement to be of the order of 0.01-0.02 ($\mu s^{-1}$).
[38] Abragam A 1961 *The Principles of Nuclear Magnetism* (Oxford University Press)
[39] URL http://musruser.psi.ch/
[40] Narath A 1967 *Phys. Rev.* **162**(2) 320–332
[41] Rega T 1991 *J. Phys. Condens. Matter* **3** 1871–1876
[42] Allodi G, De Renzi R, Agrestini S, Mazzoli C and Lees M R 2011 *Phys. Rev. B* **83**(10) 104408
[43] Alderman D W, Solum M S and Grant D M 1986 *The Journal of Chemical Physics* **84** 3717–3725